

Multiagent Deployment Over a Source

Nima Ghods, *Member, IEEE*, and Miroslav Krstic, *Member, IEEE*

Abstract—We consider the problem of deploying a group of autonomous vehicles (agents) in a formation that has higher density near the source of a measurable signal and lower density away from the source. The spatial distribution of the signal and the location of the source are unknown, but the signal is known to decay with the distance from the source. The vehicles do not have the capability of sensing their own positions, but they are capable of sensing the distance between them and their neighbors. We design a control algorithm based on a combination of two components. One component of the control law is inspired by the heat partial differential equation (PDE) and results in the agents deploying between two anchor agents. The other component of the control law is based on extremum seeking and achieves higher vehicle density around the source. By using averaging theory for PDEs, we prove that the vehicle density will be highest around the source. We also quantify the density function of the agents' deployment position. By discretizing the model with respect to the continuous agent index, we obtain decentralized control laws for discrete agents and illustrate the theoretical results with simulations.

I. INTRODUCTION

A. Motivation:

EXTREMUM seeking (ES) has proved to be a powerful tool in real-time nonmodel-based control and optimization for *single* unmanned autonomous vehicles [1]–[5]. In recent years, ES has also been used for *groups* of unmanned autonomous vehicles in a network with each vehicle having limited local information [6], [7].

B. Results of the Paper: We consider the task of seeking the maximum of a signal field while simultaneously achieving a formation distribution that has higher density around the areas with higher signal strength. We combine the method of ES with diffusion feedback to have a group of vehicles complete the task of formation deployment and source seeking.

With the new method, we explore two different types of control for the agents on the boundary, which we refer to as *anchors*: 1) the case of *free* anchors and 2) the case of *fixed* anchors. The free anchor case allows the agents on the edge of the formation to freely move, whereas the fixed anchors case has stationary anchor agents that start at a desired location. Different deployment distributions are achieved in the two cases.

The diffusion-based feedback enables the overall multiagent formation to act as a net of source seekers, rather than as a group of independent, uncoordinated seekers, who intrude upon each others' space. With the free anchors, the user casts the net

in a manner to prompt attraction toward the source and spread around the source. In the fixed anchor case, the ends of the net are fixed and the agents in between distribute such that they have the highest density near the source.

In this paper, we consider only the 1-D problem. The 2-D-coordinated source seeking problem allows a much broader array of problem formulations, depending on various possible formation topologies. For this reason, we focus on the 1-D situation to introduce the design ideas and analysis techniques.

The motivation for using the diffusion/heat partial differential equation (PDE) is that the diffusion action induces each agent to take a position half way between his two neighbors. By combining diffusion with ES, one obtains a swarm of agents where each agent is driven by two competing strategies, ES that aims to place all the agents at the extremum, and diffusion that aims to spread the agents evenly, provided that the anchors are apart. The overall result of these two effects is that the agents are deployed more densely near the extremum than away from the extremum. We quantify this density in the paper.

This paper is a journal version of [8]. Unlike in [8] where all the agents use the same gains, in this paper, the agents are allowed to use different gains.

C. Literature: The problem of understanding when the individual actions of interacting agents give rise to a coordinated behavior has received a considerable attention in many fields. In the control community, the interest in coordination phenomena has been recently promoted by the need of controlling groups of unmanned autonomous vehicles. A basic setup considers a group of n mobile agents, each one described by a dynamic system capturing the evolution of its heading angle [9] or its position and velocity [10]. When agents interact with a limited number of neighbors, one faces the problem of designing a decentralized control scheme (where each agent uses only the neighbors' information) in order to orchestrate the collective behavior.

A method often used to design and analyze decentralized controller for a group of agents is to treat the agents as a continuum. Relations between distributed consensus algorithms and the heat equation are made in [11]. Agents use model reference adaptive control laws to track desired trajectories in [12], using either the heat equation or the wave equation as reference models. Boundary control of PDEs was used to deploy vehicles into planar curves in [13]. A continuum model for a swarm of vehicles is formulated by using a vehicle density function in [14]. Deployment on a line segment is achieved by using feedback laws consistent with the spatially discretized heat equation in [15].

Multiagent and GPS-enabled source seeking problems have been solved in [16] and [17]. A hybrid strategy for solving the source seeking problem was developed in [18]. The proposed problem in this paper is considered in [19]–[21] as a GPS-enabled game problem where each agent is trying to maximize its

Manuscript received August 18, 2010; revised November 30, 2010; accepted December 30, 2010. Manuscript received in final form January 03, 2011. Date of publication January 28, 2011; date of current version December 14, 2011. Recommended by Associate Editor A. Serrani. This work was supported in part by the Los Alamos National Laboratory and Office of Naval Research (ONR).

The authors are with the Department of Mechanical and Aerospace Engineering, University of California, San Diego, La Jolla, CA 92093-0411 USA (e-mail: nghods@ucsd.edu; krstic@ucsd.edu).

Color versions of one or more of the figures in this paper are available online at <http://ieeexplore.ieee.org>.

Digital Object Identifier 10.1109/TCST.2011.2104959

own cost function, but in these algorithms, the agents also require the cost information of their neighbors. The key tool in this paper is ES [22], which has been advanced or employed in applications by several other authors [23]–[27].

D. Organization of the Paper: Section II presents a description of the vehicle model and the control scheme for both free and fixed anchor cases. We prove local exponential convergence results of an equilibrium with the density function that has maximum density set around the source in Sections III and IV. Section III deals with the case of free anchors, whereas Section IV deals with fixed anchors. Simulation results in Section V illustrate the distinct behavior exhibited using free and fixed control for the anchor agents with and without independent parameters for each agent.

II. CONTROL DESIGN

We consider vehicles modeled as a velocity-actuated point mass $x_t = v$, where x is a vector of position of the point masses and v are the vehicles velocity inputs. It is common to consider the heat equation $x_t(\alpha, t) = x_{\alpha\alpha}(\alpha, t)$ as a model that governs the position $x(\alpha, t)$ at time t of an agent indexed by α in a large (continuum) group of agents, where each agent is able to sense its nearest neighbor and applies diffusion feedback actuated through the velocity input, namely, $v(\alpha, t) = x_{\alpha\alpha}(\alpha, t)$, with the boundary conditions (BCs) at $x_t(0, t)$ and $x_t(1, t)$. The subscripts are used to denote a partial derivative in the respective variable. For simplicity, we choose the spatial domain $\alpha \in [0, 1]$.

ES on a single vehicle modeled as a velocity-actuated point mass has been studied in [2]. The control law used in [2] is

$$v(t) = a\omega \cos(\omega t) + c\xi \sin(\omega t) \quad (1)$$

$$\xi = \frac{s}{s+h}[J] \quad (2)$$

where J is the measurement of the signal field and a , ω , c , and h are the parameters chosen by the designer. The washout filter (2) is not required for stability [28], but used to achieve better performance.

In this paper, given only the measurements of the values of the function $J = f(x)$, we employ a mix of ES and nearest-neighbor-based diffusion feedback given by

$$v(\alpha, t) = \kappa(\alpha)x_{\alpha\alpha}(\alpha, t) + a(\alpha)\omega \cos(\omega t) + c(\alpha)\xi(\alpha, t) \sin(\omega t) \quad (3)$$

$$\xi(\alpha, t) = \frac{s}{s+h(\alpha)}[J(\alpha, t)] \quad (4)$$

where the performance can be influenced by the positive parameters $a(\alpha)$, $c(\alpha)$, $\kappa(\alpha)$, $h(\alpha)$, and ω . The parameters can vary with respect to α , which allow each vehicle to have different parameters.

For the agents on the boundary (anchor agents), we consider two different types of control laws. We explore first the case of having the anchors free to move according to the shape and location of the signal field, and then, consider the case where the user deploys the anchors to desired locations.

The free anchor BCs have the form

$$v(0, t) = -\kappa(0)\nu + a(0)\omega \cos(\omega t) + c(0)\xi(0, t) \sin(\omega t) \quad (5)$$

$$v(1, t) = \kappa(1)\nu + a(1)\omega \cos(\omega t) + c(1)\xi(1, t) \sin(\omega t) \quad (6)$$

where ν is a constant velocity that makes the anchors expand out until the ES term is big enough to counteract ν and stop the expansion of the anchors.

The fixed anchor BCs have the form

$$x(0, t) = \underline{x} \quad x(1, t) = \bar{x} \quad (7)$$

where \underline{x} and \bar{x} are the desired fixed locations of the boundary agents. The fixed BCs are used to force the agents in between the anchors (follower agents) to distribute between the desired locations. The fixed anchors can be virtual points whose positions are fed to the nearest followers, or the fixed anchors can represent a physical boundary like a wall that the followers can sense.

With the free anchors, there are no restrictions on where the formation will end up. The deployment range depends primarily on the initial anchor velocities ν . On the other hand, the fixed anchor case allows the user to pick an area of interest and have the agents explore all of this area.

We assume that the nonlinear map defining the distribution of the signal field is quadratic and takes the form

$$J = f(x) = f^* - q(x - x^*)^2 \quad (8)$$

where x is the position of the vehicle, x^* is the maximizer, $f^* = f(x^*)$ is the maximum, and q is an unknown positive constant. The assumption of the quadratic form for the signal field is used to simplify the stability proof.

III. FREE ANCHORS

In this section, we analyze the convergence properties of the feedback law (3)–(6). We define an output error variable $e(\alpha, t) = (h(\alpha))/(s+h(\alpha))[J(\alpha, t)] - f^*$, where $(h(\alpha))/(s+h(\alpha))$ is a low-pass filter applied to the sensor reading J , which allows us to express $\xi(\alpha, t)$, the signal from the washout filter, as $\xi(\alpha, t) = (s)/(s+h(\alpha))[J(\alpha, t)] = J(\alpha, t) - f^* - e(\alpha, t)$, noting also that $\dot{e}(\alpha, t) = h(\alpha)\xi(\alpha, t)$.

To study the vehicle formation in a continuum case, we use the formation density function

$$p(x) = \frac{d}{dx}\phi^{-1}(x) = \frac{1}{\phi'(\phi^{-1}(x))} \quad (9)$$

where the $\phi^{-1}(x)$ is the inverse function of vehicle position $\phi(\alpha)$ and ϕ' denotes the derivative with respect to the function's only argument.

Theorem 1: Consider the closed-loop system

$$x_t(\alpha, t) = \kappa(\alpha)x_{\alpha\alpha}(\alpha, t) + a(\alpha)\omega \cos(\omega t) + c(\alpha)\xi(\alpha, t) \sin(\omega t) \quad (10)$$

$$e_t(\alpha, t) = h(\alpha)\xi(\alpha, t) \quad (11)$$

$$\xi(\alpha, t) = -q(x(\alpha, t) - x^*)^2 - e(\alpha, t) \quad (12)$$

with the free BCs

$$\begin{aligned} x_i(0, t) &= -\kappa(0)\nu + a(0) \cos(\omega t) \\ &\quad + c(0)\xi(0, t) \sin(\omega t) \end{aligned} \quad (13)$$

$$\begin{aligned} x_i(1, t) &= \kappa(1)\nu + a(1) \cos(\omega t) \\ &\quad + c(1)\xi(1, t) \sin(\omega t) \end{aligned} \quad (14)$$

where $\kappa(\alpha), h(\alpha), a(\alpha), c(\alpha) > 0$ and $a(\alpha), c(\alpha)$ are chosen such that $(d)/(d\alpha)(a(\alpha)c(\alpha)) < (a(\alpha)c(\alpha))/(2) \forall \alpha \in [0, 1], q > 0$, and $\nu \in BBR$. There exists $\omega^* > 0$ such that, for all $\omega > \omega^*$, there exists a periodic solution $(x^{2\pi/\omega}(\alpha, t), e^{2\pi/\omega}(\alpha, t))$ of period $2\pi/\omega$ in t and with the property that

$$\left| x^{2\pi/\omega}(\alpha, t) - x^* - \rho(\alpha) \right|^2 \leq O\left(\frac{1}{\omega} + \max_{\alpha} a(\alpha)\right) \quad (15)$$

$\forall \alpha \in [0, 1], t \geq 0$, where

$$\rho(\alpha) = a_0^{\text{free}} e^{\gamma(\alpha)} - a_1^{\text{free}} e^{-\gamma(\alpha)} \quad (16)$$

$$a_0^{\text{free}} = \frac{\nu}{e^{\gamma(1)} - e^{-\gamma(1)}} \left(\frac{1}{\lambda^2(1)} + \frac{e^{-\gamma(1)}}{\lambda^2(0)} \right) \quad (17)$$

$$a_1^{\text{free}} = \frac{\nu}{e^{\gamma(1)} - e^{-\gamma(1)}} \left(\frac{1}{\lambda^2(1)} + \frac{e^{\gamma(1)}}{\lambda^2(0)} \right) \quad (18)$$

$$\gamma(\alpha) = \int_0^{\alpha} \lambda(\sigma) d\sigma \quad (19)$$

$$\lambda(\sigma) = \sqrt{\frac{qc(\sigma)a(\sigma)}{\kappa(\sigma)}} \quad (20)$$

such that whenever the quantities

$$\begin{aligned} &|x(0, 0) - x^* - \rho(0)|^2 \\ &\int_0^1 |x(\alpha, 0) - x^* - \rho(\alpha)|^2 d\alpha \\ &\int_0^1 |x_{\alpha}(\alpha, 0) - \rho_{\alpha}(\alpha)|^2 d\alpha \end{aligned} \quad (21)$$

$$\int_0^1 \left| e(\alpha, 0) + \frac{qa^2}{2} + q\rho^2(\alpha) \right|^2 d\alpha \quad (22)$$

are sufficiently small, the solution $(x(\alpha, t), e(\alpha, t))$ exponentially converges to $(x^{2\pi/\omega}(\alpha, t), e^{2\pi/\omega}(\alpha, t))$ in $H^1[0, 1] \times L^2[0, 1]$ norm.

Proof: We start the proof by defining the error variable

$$\tilde{x} = x - x^* - a(\alpha) \sin(\omega t) \quad (23)$$

where x^* is the location of the source, and the new time variable

$$\tau = \omega t. \quad (24)$$

The resulting dynamics become

$$\tilde{x}_{\tau}(\alpha, \tau) = \frac{1}{\omega} (\kappa(\alpha)(\tilde{x}_{\alpha\alpha}(\alpha, \tau) + a''(\alpha) \sin(\tau))$$

$$- c(\alpha)\xi(\alpha, \tau) \sin(\tau)) \quad (25)$$

$$e_{\tau}(\alpha, \tau) = \frac{h(\alpha)}{\omega} \xi(\alpha, \tau) \quad (26)$$

$$\xi(\alpha, \tau) = -q(\tilde{x}(\alpha, \tau) + a(\alpha) \sin(\tau))^2 - e(\alpha, \tau) \quad (27)$$

with BC

$$\tilde{x}_{\tau}(0, \tau) = \frac{1}{\omega} (-\kappa(0)\nu + c(0)\xi(0, \tau) \sin(\tau))$$

$$\tilde{x}_{\tau}(1, \tau) = \frac{1}{\omega} (\kappa(1)\nu + c(1)\xi(1, \tau) \sin(\tau)). \quad (28)$$

The average error system is

$$\begin{aligned} &\tilde{x}_{\tau}^{\text{ave}}(\alpha, \tau) \\ &= \frac{1}{\omega} (\kappa(\alpha)\tilde{x}_{\alpha\alpha}^{\text{ave}}(\alpha, \tau) - qc(\alpha)a(\alpha)\tilde{x}^{\text{ave}}(\alpha, \tau)) \end{aligned} \quad (29)$$

$$\begin{aligned} &e_{\tau}^{\text{ave}}(\alpha, \tau) \\ &= -\frac{h(\alpha)}{\omega} \left(q(\tilde{x}^{\text{ave}}(\alpha, \tau))^2 + \frac{qa^2(\alpha)}{2} + e^{\text{ave}}(\alpha, \tau) \right) \end{aligned} \quad (30)$$

with BC

$$\tilde{x}_{\tau}^{\text{ave}}(0, \tau) = \frac{1}{\omega} (-\kappa(0)\nu - qc(0)a(0)\tilde{x}^{\text{ave}}(0, \tau)) \quad (31)$$

$$\tilde{x}_{\tau}^{\text{ave}}(1, \tau) = \frac{1}{\omega} (\kappa(1)\nu - qc(1)a(1)\tilde{x}^{\text{ave}}(1, \tau)). \quad (32)$$

The equilibrium profile of the average error system (29)–(32) is

$$\left[\tilde{x}^{\text{ave}^e}(\alpha), e^{\text{ave}^e}(\alpha) \right] = \left[\rho(\alpha), -\frac{qa^2(\alpha)}{2} - q\rho^2(\alpha) \right] \quad (33)$$

where $\rho(\alpha)$ is given in (16).

We shift the system state by its equilibrium profile with the transformations $w(\alpha, \tau) = x^{\text{ave}}(\alpha, \tau) - x^{\text{ave}^e}(\alpha)$ and $z(\alpha, \tau) = e^{\text{ave}}(\alpha, \tau) - e^{\text{ave}^e}(\alpha)$, which results in the following dynamics:

$$\begin{aligned} &w_{\tau}(\alpha, \tau) \\ &= \frac{1}{\omega} (\kappa(\alpha)w_{\alpha\alpha}(\alpha, \tau) - qc(\alpha)a(\alpha)w(\alpha, \tau)) \end{aligned} \quad (34)$$

$$\begin{aligned} &z_{\tau}(\alpha, \tau) \\ &= -\frac{h(\alpha)}{\omega} (q(w(\alpha, \tau) + \rho(\alpha))^2 + z(\alpha, \tau) - q\rho^2(\alpha)) \\ &= -\frac{h(\alpha)}{\omega} (qw^2(\alpha, \tau) + 2q\rho(\alpha)w(\alpha, \tau) + z(\alpha, \tau)) \end{aligned} \quad (35)$$

with BC

$$\begin{aligned} w_{\tau}(0, \tau) &= \frac{1}{\omega} (-\kappa(0)\nu - qc(0)a(0)(w(0, \tau) + \rho(0))) \\ &= -\frac{qc(0)a(0)}{\omega} w(0, \tau) \end{aligned} \quad (36)$$

$$w_{\tau}(1, \tau) = \frac{1}{\omega} (\kappa(1)\nu - qc(1)a(1)(w(1, \tau) + \rho(1)))$$

$$= -\frac{qc(1)a(1)}{\omega}w(1, \tau). \quad (37)$$

Linearizing the averaged error system produces

$$w_\tau(\alpha, \tau) = \frac{1}{\omega} (\kappa(\alpha) w_{\alpha\alpha}(\alpha, \tau) - qc(\alpha)a(\alpha) w(\alpha, \tau)) \quad (38)$$

$$z_\tau(\alpha, \tau) = -\frac{h(\alpha)}{\omega} (2q\rho(\alpha)w(\alpha, \tau) + z(\alpha, \tau)) \quad (39)$$

with BC

$$w_\tau(0, \tau) = -\frac{qc(0)a(0)}{\omega}w(0, \tau) \quad (40)$$

$$w_\tau(1, \tau) = -\frac{qc(1)a(1)}{\omega}w(1, \tau). \quad (41)$$

By using Lemma A.1 in Appendix A, where $k_1 = \kappa(\alpha)$, $k_2 = qa(\alpha)c(\alpha)$, $k_3 = 2qh(\alpha)\rho(\alpha)$, and $k_4 = h(\alpha)$, we get that the averaged error system has an exponentially stable equilibrium. By applying [29, Th. 3.6, Ex. 6.4] (details in Appendix B), we can state that there exists $\omega^* > 0$ such that for all $\omega > \omega^*$, there exists a periodic solution $(x^{2\pi/\omega}(\alpha, t), e^{2\pi/\omega}(\alpha, t))$ of period $2\pi/\omega$ in t and with the property that

$$\begin{aligned} & \left| x^{2\pi/\omega}(0, t) - x^* - \rho(0) \right|^2 \\ & + \int_0^1 \left| x^{2\pi/\omega}(\alpha, t) - x^* - \rho(\alpha) \right|^2 d\alpha \\ & + \int_0^1 \left| x_\alpha^{2\pi/\omega}(\alpha, t) - \rho'(\alpha) \right|^2 d\alpha \\ & \leq O\left(\frac{1}{\omega} + \max_\alpha a(\alpha)\right) \end{aligned} \quad (42)$$

so that the solution $(x(\alpha, t), e(\alpha, t))$ locally exponentially converges to $(x^{2\pi/\omega}(\alpha, t), e^{2\pi/\omega}(\alpha, t))$ in $H^1[0, 1] \times L^2[0, 1]$ norm. Agmon's inequality combined with Young's inequality yields

$$\begin{aligned} \sup_\alpha |\zeta(\alpha, t)|^2 & \leq \zeta^2(0, t) + \int_0^1 |\zeta(\alpha, t)|^2 d\alpha \\ & + \int_0^1 |\zeta_\alpha(\alpha, t)|^2 d\alpha. \end{aligned} \quad (43)$$

By applying (43) to (42), we get the bound (15). ■

Now, we take a look at how the parameters affect the density function.

Proposition 2: The averaged equilibrium (16)–(20) has the following formation density function

$$p(x) = \frac{1 + (x - x^*)/(\sqrt{(x - x^*)^2 + 4a_0a_1})}{\lambda(\phi^{-1}(x)) \left(x - x^* + \sqrt{(x - x^*)^2 + 4a_0a_1} \right)} \quad (44)$$

where $a_0 = a_0^{\text{free}}$ and $a_1 = a_1^{\text{free}}$ are given in (17) and (18).

Proof: We start by taking the vehicle position function that has the form

$$x = \phi(\alpha) = \rho(\alpha) + x^* = a_0 e^{\gamma(\alpha)} - a_1 e^{-\gamma(\alpha)} + x^* \quad (45)$$

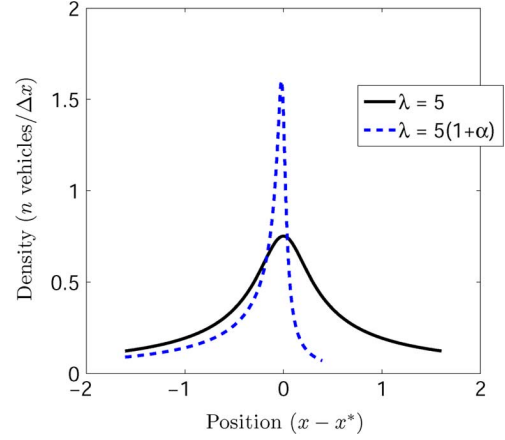


Fig. 1. Vehicle density function for $\lambda = 5$ and $\lambda(\alpha) = 5(2 - \alpha)$.

and solving (45) for γ to obtain

$$\gamma(\alpha) = \ln \left(\frac{x - x^* + \sqrt{(x - x^*)^2 + 4a_0a_1}}{a_0} \right). \quad (46)$$

We use (19) to rewrite γ in terms of λ and differentiate both sides with respect to x to obtain

$$\begin{aligned} & \left(\frac{d}{dx} \phi^{-1}(x) \right) \lambda(\phi^{-1}(x)) \\ & = \frac{1 + (x - x^*)/(\sqrt{(x - x^*)^2 + 4a_0a_1})}{\left(x - x^* + \sqrt{(x - x^*)^2 + 4a_0a_1} \right)} \end{aligned} \quad (47)$$

and then, simply solve for density function $p(x) = (d)/(dx)\phi^{-1}(x)$. ■

Note that since $\phi(\alpha)$ is monotonic, there always exists an inverse function $\phi^{-1}(x)$.

Fig. 1 shows two density plots with the parameters chosen in a way to make $\lambda = 5$ for the solid black line and $\lambda(\alpha) = 5(2 - \alpha)$ for the dashed blue line with $\nu = 2$ and $x^* = 0$ for both. Fig. 1 shows that the vehicles with higher value of $\lambda(\alpha)$ squeeze toward the maximum x^* and the vehicles with lower values of $\lambda(\alpha)$ spread out more.

We consider the simple case of constant λ to show the effect of λ and ν on the density function at x^* . The formula for density function at x^* with constant λ is given by $p(x^*) = (\sqrt{\kappa}\lambda \sinh(\lambda))/(\nu\sqrt{2 + 2\cosh(\lambda)})$, where it can be noted that as λ increases so does the density function at x^* , while the opposite is true for ν .

IV. FIXED ANCHORS

In this section, we highlight the differences in the analysis of the fixed anchor case from the free anchor case. The main differences between the two cases are that the fixed anchor case forces the formation deployment profile to be between \underline{x} and \bar{x} , which, in turn, causes the density function to be in the same range. Unlike in the free anchor case, in the fixed anchor case, the anchors are stationary.

Theorem 3: Consider the system (10)–(12) with the fixed BCs

$$x(0, t) = \underline{x} \quad x(1, t) = \bar{x} \quad (48)$$

where \underline{x} and $\bar{x} \in BBR$. There exists $\omega^* > 0$ such that for all $\omega > \omega^*$, there exists a periodic solution $(x^{2\pi/\omega}, e^{2\pi/\omega}(\alpha, t))$ of period $2\pi/\omega$ in t and with the property that

$$\left| x^{2\pi/\omega}(\alpha, t) - x^* - \rho(\alpha) \right|^2 \leq O\left(\frac{1}{\omega} + \max_{\alpha} a(\alpha)\right) \quad (49)$$

$\forall \alpha \in [0, 1], t \geq 0$, where

$$\rho(\alpha) = a_0^{\text{fixed}} e^{\gamma(\alpha)} - a_1^{\text{fixed}} e^{-\gamma(\alpha)} \quad (50)$$

$$a_0^{\text{fixed}} = \frac{\bar{x} - x^* (1 - e^{-\gamma(1)}) - \underline{x} e^{-\gamma(1)}}{(e^{\gamma(1)} - e^{-\gamma(1)})} \quad (51)$$

$$a_1^{\text{fixed}} = \frac{\bar{x} - x^* (1 - e^{\gamma(1)}) - \underline{x} e^{\gamma(1)}}{(e^{\gamma(1)} - e^{-\gamma(1)})} \quad (52)$$

and γ given by (19) such that whenever the quantities

$$\int_0^1 |x(\alpha, 0) - x^* - \rho(\alpha)|^2 d\alpha + \int_0^1 \left| e(\alpha, 0) + \frac{qa^2}{2} + q\rho^2(\alpha) \right|^2 d\alpha \quad (53)$$

are sufficiently small, the solution $(x(\alpha, t), e(\alpha, t))$ exponentially converges to $(x^{2\pi/\omega}(\alpha, t), e^{2\pi/\omega}(\alpha, t))$ in $L^2[0, 1] \times L^2[0, 1]$ norm.

Proof: Similar to the proof for Theorem 1, we start by applying (23) and (24) to system (10) and (12) with the BC (48), and then, by averaging, we obtain

$$\begin{aligned} \tilde{x}_{\tau}^{\text{ave}}(\alpha, \tau) &= \frac{1}{\omega} (\kappa(\alpha) \tilde{x}_{\alpha\alpha}^{\text{ave}}(\alpha, \tau) - qc(\alpha) a(\alpha) \tilde{x}^{\text{ave}}(\alpha, \tau)) \quad (54) \\ e_{\tau}^{\text{ave}}(\alpha, \tau) &= -\frac{h(\alpha)}{\omega} \left(q(\tilde{x}^{\text{ave}}(\alpha, \tau))^2 + \frac{qa(\alpha)^2}{2} + e^{\text{ave}}(\alpha, \tau) \right) \quad (55) \end{aligned}$$

with BC

$$\tilde{x}^{\text{ave}}(0, \tau) = \underline{x} - x^* \quad \tilde{x}^{\text{ave}}(1, \tau) = \bar{x} - x^*. \quad (56)$$

The average error system (54)–(56) has an equilibrium $[\tilde{x}^{\text{ave}}(\alpha), e^{\text{ave}}(\alpha)] = [\rho(\alpha), -(qa^2)/(2) - q\rho^2(\alpha)]$, where $\rho(\alpha)$ is given in (50). We omit the details of the averaging, but would like to point out that the main difference in averaging the fixed case from the free case is in the BC that makes the equilibrium (50) have different coefficients.

By shifting the averaged system by the equilibrium and linearizing, we get

$$w_{\tau}(\alpha, \tau) = \frac{1}{\omega} (\kappa(\alpha) w_{\alpha\alpha}(\alpha, \tau) - qc(\alpha) a(\alpha) w(\alpha, \tau)) \quad (57)$$

$$z_{\tau}(\alpha, \tau) = -\frac{h(\alpha)}{\omega} (2q\rho(\alpha) w(\alpha, \tau) + z(\alpha, \tau)) \quad (58)$$

with BC, $w(0, \tau) = w(1, \tau) = 0$.

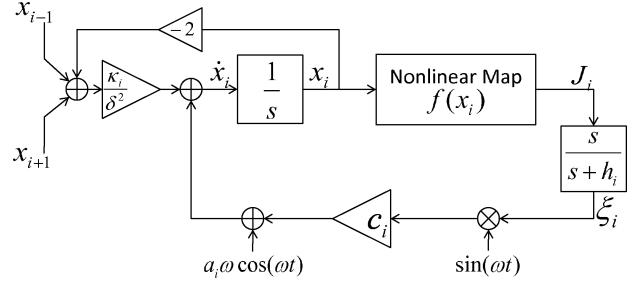


Fig. 2. Block diagram of a single follower agent.

By using Lemma A.3 in Appendix A, where $k_1 = \kappa(\alpha)$, $k_2 = qa(\alpha)c(\alpha)$, $k_3 = 2qh(\alpha)\rho(\alpha)$, and $k_4 = h(\alpha)$, we get that the averaged error system has an exponentially stable equilibrium. By using [29, Theorem 3.6 and Example 6.4] (details in Appendix B), we can state that there exists $\omega^* > 0$ such that for all $\omega > \omega^*$, there exists a periodic solution $(x^{2\pi/\omega}, e^{2\pi/\omega}(\alpha, t))$ of period $2\pi/\omega$ in t and with the property that

$$\int_0^1 \left| x^{2\pi/\omega}(\alpha, t) - x^* - \rho(\alpha) \right|^2 d\alpha \leq O\left(\frac{1}{\omega} + \max_{\alpha} a(\alpha)\right) \quad (59)$$

so that the solution $(x(\alpha, t), e(\alpha, t))$ locally exponentially converges to $(x^{2\pi/\omega}(\alpha, t), e^{2\pi/\omega}(\alpha, t))$ in $L^1[0, 1] \times L^2[0, 1]$ norm. By applying (43) to (59), we get the bound (49). ■

The same result holds as in Proposition 2 for the averaged equilibrium of the fixed anchor case (50)–(52) with the formation density function given as (44) where $a_0 = a_0^{\text{fixed}}$ and $a_1 = a_1^{\text{fixed}}$ are given in (51) and (52), respectively. As derived earlier, the formation density function at position x^* with a constant λ , given by $p(x^*) = (\sinh(\lambda))/(\lambda\beta)$, where $\beta = (x^{*2} - x^*(\underline{x} + \bar{x}))(2 - 2\cosh(\lambda)) - 2\underline{x}\bar{x}\cosh(\lambda) + \bar{x}^2 + \underline{x}^2$ increases with bigger λ and decreases as the difference between \underline{x} and \bar{x} grows.

V. SIMULATION RESULTS

To implement the algorithm in Section II, we must first understand how to choose and tune the parameters a , c , κ , ω , h , and ν . Higher values of a and c cause the attraction of the vehicle toward the source to increase and the opposite is true for κ . The parameters ω and a are chosen such that the quantity $1/\omega + \max_{\alpha} a(\alpha)$ is sufficiently small. The cutoff frequency h for the washout filter has to be high enough to significantly get rid of the dc term but smaller than the perturbation frequency ω . In the free anchor case, the higher the ratio $\nu\kappa/ac$, the farther the anchor vehicle will settle from the source, thereby causing the formation to spread out.

We discretize the continuous model (3) to implement the algorithm. The two anchor agents do not require any modification of their control laws (5)–(7) since they do not include any partial differentiation with respect to the agent index in their control law. The state variables $x(\alpha, t)$ and $\xi(\alpha, t)$ become $x(i\delta, t)$ and $\xi(i\delta, t)$, where $i = 0, \dots, n$, $\delta = 1/n$, and $n + 1$ is the number of agents. We denote the two anchor agents' states as $[x_0, \xi_0]$ and $[x_n, \xi_n]$, and the interior seeking agents' states as $[x_i, \xi_i]$.

We discretize the seeking agents' control laws (3) by using three-point central differencing to approximate the spatial

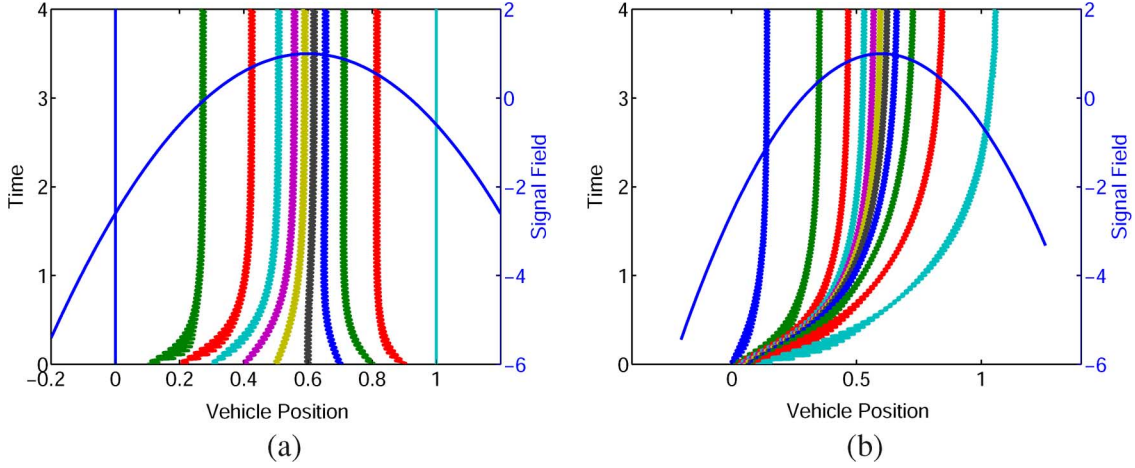


Fig. 3. Double y-axis plots of the vehicle trajectories, showing time scale on the left y-axis, the signal field strength on the right y-axis, and the location of the vehicles on the x-axis. (a) Agent deployment with fixed anchors. (b) Agent deployment with free anchors.

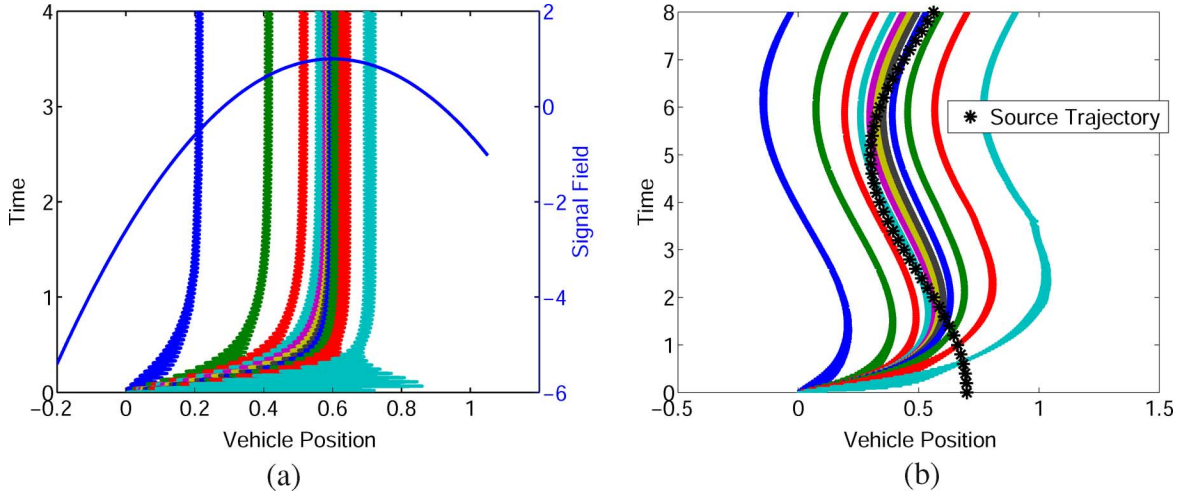


Fig. 4. (a) Agent deployment with free anchors starting far from the equilibrium with linearly increasing parameters a and c . (b) Group of 11 agents using free anchor case to achieve seeking of a moving source.

derivatives, obtaining $v_i(t) = \kappa_i(x_{i+1} - 2x_i + x_{i-1})/(\delta^2) + a_i \cos(\omega t) + c_i \xi_i(t) \sin(\omega t)$, which can be rearranged as

$$v_i(t) = \kappa_i \frac{\Delta x_{i+1,i} + \Delta x_{i-1,i}}{\delta^2} + a_i \cos(\omega t) + c_i \xi_i(t) \sin(\omega t) \quad (60)$$

where $\Delta x_{j,i} = x_j - x_i$. The washout filter becomes $\xi_i(t) = (s)/(s+h)[J_i(t)]$, where J_i is the sensor reading of agent i . Fig. 2 shows the block diagram for one follower agent.

The signal field parameters for plots in Fig. 3 are $f^* = 1$, $q = 10$, and $x^* = 0.6$. We apply (60), where $a = 0.008$, $c = 15$, $\kappa = 0.05$, $\omega = 45$, and $h = 10$, for all follower agents and $x_0 = 0$, $x_n = 1$ for the anchor agents to simulate the fixed agent case on 11 agents. Fig. 3(a) shows the evolution of a group of autonomous vehicles, with fixed boundary agents, all released equidistantly between x_0 and x_n . The agents deploy more densely around the signal source (peak) than away from the source that is consistent with the form of the density function (44), where $a_0 = a_0^{\text{fixed}}$ and $a_1 = a_1^{\text{fixed}}$ are given in (51) and (52), respectively.

We simulate the free BC case by using

$$v_n(t) = -\kappa\nu + a\omega \cos(\omega t) + c\xi_0(t) \sin(\omega t) \quad (61)$$

$$v_n(t) = \kappa\nu + a\omega \cos(\omega t) + c\xi_n(t) \sin(\omega t) \quad (62)$$

and (60), where a , c , κ , ω , and h have the same value as the first simulation and $\nu = 0.5$. Fig. 3(b) shows the evolution of a group of 11 autonomous vehicles, with free boundary control, released starting with the anchor agents at position 0 and 0.1 and the follower agents spread equally between them. The deployment density is consistent with the theoretically predicted solid curve in Fig. 1.

The simulation in Fig. 4 is produced with the same parameters as the simulation shown in Fig. 3(b), except that in Fig. 4(a), the ES parameters $a_i = 0.008(1 + i/n)$, $c_i = 15(1 + i/n)$ and, in Fig. 4(b), the source is moving according to $x^*(t) = c_{x^*} + a_{x^*} \sin(\omega_{x^*} t)$, where $c_{x^*} = 0.6$, $a_{x^*} = 0.2$, and $\omega_{x^*} = \pi/5$. Fig. 4(a) shows how the increasing of the parameters a and c with respect to the agents index i pulls the agents with a higher i closer to the source. Fig. 4(b) shows how the algorithm handles a moving source.

VI. CONCLUSION

We have introduced algorithms that expand the capability of previous single-agent source seeking algorithms. The new multiagent source seeking algorithms cover the area around the source in such a manner that the highest density of agents is

achieved at the source and the density decreases away from the source. This form of deployment is achieved by combining standard ES with consensus-type ideas, namely, by using algorithms that are simultaneously driven by the local signal strength and diffusion feedback, which employs the distance to the nearest agents. While diffusion aims to place an agent exactly halfway between its neighbors, ES aims to pull the agent closer to the source. In the presence of anchor agents that deploy some distance apart, the result is that agents deploy more densely near the source than away from the source.

Of interest for future research is to extend the present algorithms to the stochastic case, namely, to replace the sinusoidally forced ES algorithms by ES algorithms forced by white noise [5]. In addition, it is of interest to extend the current results for 1-D formations in 1-D space to higher dimensional formations in higher dimensional space. Finally, it is of interest to extend the present results to nonholonomic vehicles.

APPENDIX A TECHNICAL LEMMAS

Lemma A.1: Consider the following system

$$w_\tau(\alpha, \tau) = k_1(\alpha)w_{\alpha\alpha}(\alpha, \tau) - k_2(\alpha)w(\alpha, \tau) \quad (63)$$

$$z_\tau(\alpha, \tau) = -k_3(\alpha)z(\alpha, \tau) - k_4(\alpha)w(\alpha, \tau) \quad (64)$$

with BCs

$$w_\tau(0, \tau) = -k_2(0)w(0, \tau) \quad w_\tau(1, \tau) = -k_2(1)w(1, \tau) \quad (65)$$

where $k_1(\alpha), k_2(\alpha), k_3(\alpha)$, and $k_4(\alpha)$ are strictly positive bounded functions, and $k_2'(\alpha) < (1)/(2)k_2(\alpha) \forall \alpha \in [0, 1]$. The system (63)–(65) is exponentially stable at the equilibrium $w = 0, z = 0$, i.e., there exists $M > 0$ and $\mu > 0$ such that for all $\tau > 0$

$$\Omega(\tau) \leq M e^{-\mu\tau} \Omega(0) \quad (66)$$

where

$$\begin{aligned} \Omega(\tau) = & \int_0^1 w(\alpha, \tau)^2 d\alpha + \int_0^1 w_\alpha(\alpha, \tau)^2 d\alpha + w(0, \tau)^2 \\ & + \int_0^1 z(\alpha, \tau)^2 d\alpha. \end{aligned} \quad (67)$$

Proof: Let $V(\tau)$ be the Lyapunov functional

$$\begin{aligned} V(\tau) = & \frac{m}{2} \int_0^1 w_\alpha(\alpha, \tau)^2 d\alpha + \frac{m}{2} w(0, \tau)^2 \\ & + \frac{1}{2} \int_0^1 z(\alpha, \tau)^2 d\alpha \end{aligned} \quad (68)$$

where m is a positive scalar to be determined. Computing the derivative of $V(\tau)$ gives

$$\begin{aligned} \dot{V} = & m \int_0^1 w_{\tau\alpha}(\alpha, \tau)w_\alpha(\alpha, \tau) d\alpha + mw_\tau(0, \tau)w(0, \tau) \\ & + \int_0^1 z_\tau z d\alpha. \end{aligned} \quad (69)$$

By integrating the first term by parts, we obtain

$$\begin{aligned} \dot{V} = & mw_\tau w_\alpha|_0^1 - m \int_0^1 w_\tau(\alpha, \tau)w_{\alpha\alpha}(\alpha, \tau) d\alpha \\ & + w_\tau(0, \tau)w(0, \tau) + \int_0^1 z_\tau(\alpha, \tau)z(\alpha, \tau) d\alpha. \end{aligned} \quad (70)$$

Substituting (63)–(65) yields

$$\begin{aligned} \dot{V} = & -mk_2(\alpha)w(\alpha, \tau)w_\alpha(\alpha, \tau)|_0^1 \\ & - m \int_0^1 k_1(\alpha)w_{\alpha\alpha}(\alpha, \tau)^2 d\alpha \\ & + m \int_0^1 k_2(\alpha)w(\alpha, \tau)w_{\alpha\alpha}(\alpha, \tau) d\alpha \\ & - mk_2(0)w(0, \tau)^2 - \int_0^1 k_3(\alpha)z(\alpha, \tau)^2 d\alpha \\ & - \int_0^1 k_4(\alpha)\rho(\alpha)w(\alpha, \tau)z(\alpha, \tau) d\alpha. \end{aligned} \quad (71)$$

The second term is negative and can be removed. Integrating by parts on the third term of (71) gives

$$\begin{aligned} \dot{V} \leq & -m \int_0^1 k_2(\alpha)w_\alpha(\alpha, \tau)^2 d\alpha - mk_2(0)(w(0, \tau))^2 \\ & - m \int_0^1 k_2'(\alpha)w(\alpha, \tau)w_\alpha(\alpha, \tau) d\alpha \\ & - \int_0^1 k_3(\alpha)z(\alpha, \tau)^2 d\alpha \\ & - \int_0^1 k_4(\alpha)w(\alpha, \tau)z(\alpha, \tau) d\alpha. \end{aligned} \quad (72)$$

We now bound \dot{V} by applying the Cauchy–Schwarz and Young’s inequality to the third and last terms with the parameters $\theta_1, \theta_2 > 0$

$$\begin{aligned} \dot{V} \leq & -m \int_0^1 k_2(\alpha)w_\alpha(\alpha, \tau)^2 d\alpha - mk_2(0)w(0, \tau)^2 \\ & - \int_0^1 k_3(\alpha)z(\alpha, \tau)^2 d\alpha + \frac{1}{2\theta_1} \int_0^1 z(\alpha, \tau)^2 d\alpha \\ & + \frac{m}{2\theta_2} \int_0^1 k_2'(\alpha) d\alpha \int_0^1 w_\alpha(\alpha, \tau)^2 d\alpha \\ & + \frac{m}{2} \int_0^1 \left(\frac{\theta_1}{m} k_4^2(\alpha) + \theta_2 k_2'(\alpha) \right) d\alpha \\ & \times \int_0^1 w(\alpha, \tau)^2 d\alpha. \end{aligned} \quad (73)$$

By applying Poincare inequality in the last term that states $\int_0^1 w(\alpha, \tau)^2 d\alpha \leq 2w(0, \tau)^2 + 4 \int_0^1 w_\alpha(\alpha, \tau)^2 d\alpha$, letting $\underline{k}_2 = \min_{\alpha \in [0, 1]} (k_2(\alpha) - 2k_2'(\alpha))$, $\underline{k}_3 = \min_{\alpha \in [0, 1]} k_3(\alpha)$, $\bar{k}_4 = \max_{\alpha \in [0, 1]} k_4(\alpha)$, and choosing $\theta_1 = 1/\underline{k}_3$ and $\theta_2 = 1/2$, we get

$$\begin{aligned} \dot{V} \leq & -m \left(\underline{k}_2 - 2 \frac{\bar{k}_4^2}{m \underline{k}_3} \right) \int_0^1 w_\alpha(\alpha, \tau)^2 d\alpha \\ & - m \left(\underline{k}_2 - \frac{\bar{k}_4^2}{m \underline{k}_3} \right) w(0, \tau)^2 - \frac{\underline{k}_3}{2} \int_0^1 z(\alpha, \tau)^2 d\alpha. \end{aligned} \quad (74)$$

By selecting the analysis parameters $m = 4(\bar{k}_4)/(k_2 k_3)$, we find

$$\begin{aligned} \dot{V} &\leq -\frac{m\mu}{2} \int_0^1 w_\alpha(\alpha, \tau)^2 d\alpha - \frac{m\mu}{2} w(0, \tau)^2 - \frac{\mu}{2} \int_0^1 z(\alpha, \tau)^2 d\alpha \\ &\leq -\mu V \end{aligned} \quad (75)$$

where $\mu = \min(k_2, k_3)$. From the comparison lemma [30] and Lemma A.2, we have

$$\Omega(\tau) \leq \frac{1}{p_1} V(\tau) \leq \frac{1}{p_1} e^{-\mu\tau} V(0) \leq \frac{p_2}{p_1} e^{-\mu\tau} \Omega(0) \quad (76)$$

where $p_1 = (1)/(2) \min((m)/(8), 1)$ and $p_2 = (1)/(2) \max(m, 1)$. The result (66) is obtained from (76) with $M = (p_2)/(p_1)$. ■

Lemma A.2: There exists p_1 and $p_2 > 0$ such that

$$p_1 \Omega(\tau) \leq V(\tau) \leq p_2 \Omega(\tau) \quad (77)$$

where $\Omega(\tau)$ and $V(\tau)$ are shown (67) and (68), respectively.

Proof: With $p_2 = (1)/(2) \max(m, 1)$, the RHS of the (77) is immediate. Rewriting $V(\tau)$ by using Poincare inequality

$$\begin{aligned} V(\tau) &\geq \frac{m}{4} \int_0^1 w_\alpha(\alpha, \tau)^2 d\alpha + \frac{m}{16} \int_0^1 w(\alpha, \tau)^2 d\alpha \\ &\quad + \frac{3m}{8} w(0, \tau)^2 + \frac{1}{2} \int_0^1 z(\alpha, \tau)^2 d\alpha \end{aligned} \quad (78)$$

we obtain the LHS of (77), with $p_1 = (1)/(2) \min((m)/(8), 1)$. ■

Lemma A.3: Consider the following system:

$$w_\tau(\alpha, \tau) = k_1(\alpha) w_{\alpha\alpha}(\alpha, \tau) - k_2(\alpha) w(\alpha, \tau) \quad (79)$$

$$z_\tau(\alpha, \tau) = -k_3(\alpha) z(\alpha, \tau) - k_4(\alpha) w(\alpha, \tau) \quad (80)$$

with BCs, $w(0, \tau) = 0$ and $w(1, \tau) = 0$, where $k_1(\alpha), k_2(\alpha), k_3(\alpha)$, and $k_4(\alpha)$ are strictly positive bounded functions $\forall \alpha \in [0, 1]$. The system (79)–(80) is exponentially stable at the equilibrium $w = 0, z = 0$, i.e., there exists $\mu > 0$ such that for all $\tau > 0$

$$V(\tau) \leq e^{-\mu\tau} V(0) \quad (81)$$

where $V(\tau) = (1)/(2) \int_0^1 (mw(\alpha, \tau)^2)/(k_1(\alpha)) d\alpha + (1)/(2) \int_0^1 z(\alpha, \tau)^2 d\alpha$ and $m > 0$ is given in the proof.

Proof: Computing the derivative of V gives us

$$\dot{V} = - \int_0^1 \frac{m}{k_1(\alpha)} w_\tau(\alpha, \tau) w(\alpha, \tau) d\alpha - \int_0^1 z_\tau(\alpha, \tau) z(\alpha, \tau) d\alpha \quad (82)$$

and by substituting (79) and (80), we obtain

$$\begin{aligned} \dot{V} &= m \int_0^1 w_{\alpha\alpha}(\alpha, \tau) w(\alpha, \tau) d\alpha \\ &\quad - m \int_0^1 \frac{k_2(\alpha)}{k_1(\alpha)} w(\alpha, \tau)^2 d\alpha \\ &\quad - \int_0^1 k_3(\alpha) z(\alpha, \tau)^2 d\alpha \\ &\quad - \int_0^1 k_4(\alpha) w(\alpha, \tau) z(\alpha, \tau) d\alpha. \end{aligned} \quad (83)$$

By integrating by parts on the first term and using the Cauchy–Schwarz and Young’s inequality with the parameter $\theta > 0$ on the last term, we get

$$\begin{aligned} \dot{V} &= mw(\alpha, \tau) w_\alpha(\alpha, \tau) \Big|_0^1 - m \int_0^1 w_\alpha(\alpha, \tau)^2 d\alpha \\ &\quad - m \int_0^1 \frac{k_2(\alpha)}{k_1(\alpha)} w(\alpha, \tau)^2 d\alpha \\ &\quad - \int_0^1 k_3(\alpha) z(\alpha, \tau)^2 d\alpha \\ &\quad + \int_0^1 \frac{\theta k_4^2}{2} w(\alpha, \tau)^2 d\alpha \\ &\quad + \int_0^1 \frac{1}{2\theta} (\alpha) z(\alpha, \tau)^2 d\alpha. \end{aligned} \quad (84)$$

Given the BCs, the first term is zero. The second term is negative and can be removed. By combining the common terms, we get

$$\begin{aligned} \dot{V} &\leq - \int_0^1 \frac{m}{k_1(\alpha)} \left(k_2(\alpha) - \frac{\theta k_1(\alpha) k_4^2(\alpha)}{2m} \right) w(\alpha, \tau)^2 d\alpha \\ &\quad - \int_0^1 \left(k_3(\alpha) - \frac{1}{2\theta} \right) z(\alpha, \tau)^2 d\alpha. \end{aligned} \quad (85)$$

Letting $\bar{k}_1 = \max_{\alpha \in [0, 1]} k_1(\alpha)$, $\bar{k}_2 = \min_{\alpha \in [0, 1]} k_2(\alpha)$, $\bar{k}_3 = \min_{\alpha \in [0, 1]} k_3(\alpha)$, $\bar{k}_4 = \max_{\alpha \in [0, 1]} k_4(\alpha)$, and choosing $\theta_1 = 1/\bar{k}_3$ and $m = (\bar{k}_1 \bar{k}_4)/(k_2 k_3)$, we get

$$\begin{aligned} \dot{V} &\leq -\frac{m}{2} \bar{k}_2 \int_0^1 \frac{w(\alpha, \tau)^2}{k_1(\alpha)} d\alpha \\ &\quad - \frac{1}{2} \bar{k}_3 \int_0^1 z(\alpha, \tau)^2 d\alpha \\ &\leq -\mu V \end{aligned} \quad (86)$$

where $\mu = \min(\bar{k}_2, \bar{k}_3)$. By solving (86) for $V(\tau)$, we get (81). ■

APPENDIX B

AVERAGING IN INFINITE DIMENSIONS

We rewrite the system as $\dot{u} = \mathcal{A}u + F(t/\epsilon, u)$ with $\epsilon = 1/\omega$. For PDE system (10)–(14) with dynamic BC, $u = (\tilde{x}, e, x_l, x_r)^T$, and the operators are given as $\mathcal{A} = \text{diag}(A_0, L, 0, 0)$ with the domain of $\mathcal{D}(\mathcal{A}) = \{u \in \mathcal{D}(A_0) \times L_2(0, 1) \times BBR^2 \mid B_l \tilde{x} = x_l \text{ and } B_r \tilde{x} = x_r\}$ and $F = (F_1, F_2, F_3, F_4)^T$, where

$$\begin{aligned} A_0 f(\alpha) &= \kappa(\alpha) \frac{d^2 f(\alpha)}{d\alpha^2} \\ \mathcal{D}(A_0) &= \left\{ f(\alpha) \in L_2(0, 1) : f(\alpha) \right. \\ &\quad \left. \frac{df(\alpha)}{d\alpha} \text{ are abs. cont.}, \right. \\ &\quad \left. \frac{d^2 f(\alpha)}{d\alpha^2} \in L_2(0, 1) \right\} \end{aligned} \quad (87)$$

$$L f(\alpha) = -h(\alpha) f(\alpha), \mathcal{D}(L) = L_2(0, 1) \quad (88)$$

$$\begin{aligned} B_l f(\alpha) &= f(0), \mathcal{D}(B_l) \\ &= \{f(\alpha) \in L_2(0,1) : f(\alpha) \text{ is abs. cont.}\} \end{aligned} \quad (89)$$

$$\begin{aligned} B_r f(\alpha) &= f(1), \mathcal{D}(B_r) \\ &= \{f(\alpha) \in L_2(0,1) : f(\alpha) \text{ is abs. cont.}\} \end{aligned} \quad (90)$$

$$\begin{aligned} F_1(\omega t, \tilde{x}, e)(\alpha) &= \kappa(\alpha) a''(\alpha) \sin(\omega t) \\ &\quad - c(\alpha) \xi(\omega t, \tilde{x}, e)(\alpha) \sin(\omega t) \end{aligned} \quad (91)$$

$$F_2(\omega t, \tilde{x}, e)(\alpha) = -q(\tilde{x}(\alpha) + a(\alpha) \sin(\omega t))^2 \quad (92)$$

$$\begin{aligned} F_3(\omega t, \tilde{x}, e) &= -\nu + \kappa(0) a''(0) \sin(\omega t) \\ &\quad - c(0) \xi(\omega t, \tilde{x}, e)(0) \sin(\omega t) \end{aligned} \quad (93)$$

$$\begin{aligned} F_4(\omega t, \tilde{x}, e) &= \nu + \kappa(1) a''(1) \sin(\omega t) \\ &\quad - c(1) \xi(\omega t, \tilde{x}, e)(1) \sin(\omega t) \end{aligned} \quad (94)$$

$$\xi(\omega t, \tilde{x}, e)(\alpha) = -q(\tilde{x}(\alpha) + a(\alpha) \sin(\omega t))^2 - e(\alpha). \quad (95)$$

Similarly, for the PDE system (10)–(12) and (48) with Dirichlet BC, $u = (\tilde{x}, e)^T$ and the operators are given as $\mathcal{A} = \text{diag}(A_0, L)$ with the domain of $\mathcal{D}(\mathcal{A}) = \{u \in \mathcal{D}(A_0) \times L_2(0,1) | B_l \tilde{x} = 0 \text{ and } B_r \tilde{x} = 0\}$ and $F = (F_1, F_2)^T$, where A_0, L, B_l, B_r, F_1 , and F_2 are given in (87)–(92).

For both cases, the linear operator \mathcal{A} generates an analytic semigroup and F is periodic in t and continuously differentiable; therefore, the conditions needed to apply [29, Theorems 3.6] are satisfied.

REFERENCES

- [1] C. Zhang, D. Arnold, N. Ghods, A. Siranosian, and M. Krstic, "Source seeking with nonholonomic unicycle without position measurement and with tuning of forward velocity," *Syst. Control Lett.*, vol. 56, pp. 245–252, 2007.
- [2] C. Zhang, A. Siranosian, and M. Krstic, "Extremum seeking for moderately unstable systems and for autonomous vehicle target tracking without position measurements," *Automatica*, vol. 43, pp. 1832–1839, 2007.
- [3] J. Cochran and M. Krstic, "Source seeking with a nonholonomic unicycle without position measurements and with tuning of angular velocity part I: Stability analysis," *IEEE Trans. Autom. Control*, vol. 54, no. 4, pp. 717–731, Dec. 2009.
- [4] J. Cochran, A. Siranosian, N. Ghods, and M. Krstic, "3D source seeking for underactuated vehicles without position measurement," *IEEE Trans. Robot.*, vol. 25, no. 1, pp. 117–129, Feb. 2009.
- [5] S. J. Liu and M. Krstic, "Stochastic source seeking for nonholonomic unicycle," *Automatica*, vol. 46, pp. 1443–1453, 2010.
- [6] M. S. Stankovic and D. M. Stipanovic, "Stochastic extremum seeking with applications to mobile sensor networks," in *Proc. Amer. Control Conf.*, 2009, pp. 5622–5627.
- [7] M. S. Stankovic, K. H. Johansson, and D. M. Stipanovic, "Distributed seeking of nash equilibria with applications to mobile sensor networks," *IEEE Trans. Autom. Control*, to be published.
- [8] N. Ghods and M. Krstic, "Multi-agent deployment around a source in one dimension by extremum seeking," in *Proc. Amer. Control Conf.*, 2010, pp. 4794–4799.
- [9] A. Jadbabaie, J. Lin, and A. S. Morse, "Coordination of groups of mobile autonomous agents using nearest neighbor rules," *IEEE Trans. Autom. Control*, vol. 48, no. 6, pp. 988–1001, Jun. 2003.
- [10] H. Tanner, A. Jadbabaie, and G. Pappas, "Flocking in fixed and switching networks," *IEEE Trans. Autom. Control*, vol. 52, no. 5, pp. 863–868, May 2007.
- [11] G. Ferrari-Trecate, A. Buffa, and M. Gati, "Analysis of coordination in multi-agent systems through partial difference equations," *IEEE Trans. Autom. Control*, vol. 51, no. 6, pp. 1058–1063, Jun. 2006.
- [12] J. Kim, K.-D. Kim, V. Natarajan, S. D. Kelly, and J. Bentsman, "PDE-based model reference adaptive control of uncertain heterogeneous multiagent networks," *Nonlinear Anal.: Hybrid Syst.*, vol. 2, no. 4, pp. 1152–1167, 2008.
- [13] P. Frihauf and M. Krstic, "Leader-enabled deployment into planar curves," *IEEE Trans. Autom. Control*, to be published.
- [14] E. W. Justh and P. S. Krishnaprasad, "Equilibria and steering laws for planar formations," *Syst. Control Lett.*, vol. 52, no. 1, pp. 25–38, 2004.
- [15] R. Carli and F. Bullo, "Quantized coordination algorithms for rendezvous and deployment," *SIAM J. Control Optim.*, vol. 48, no. 3, pp. 1251–1274, 2009.
- [16] P. Ogren, E. Fiorelli, and N. Leonard, "Cooperative control of mobile sensor networks: Adaptive gradient climbing in a distributed environment," *IEEE Trans. Autom. Control*, vol. 29, no. 8, pp. 1292–1302, Aug. 2004.
- [17] B. Porat and A. Neohorai, "Localizing vapor-emitting sources by moving sensors," *IEEE Trans. Signal Process.*, vol. 44, no. 4, pp. 1018–1021, Apr. 1996.
- [18] C. G. Mayhew, R. G. Sanfelice, and A. Teel, "Robust source-seeking hybrid controllers for nonholonomic vehicles," in *Proc. Amer. Control Conf.*, Jun. 2008, pp. 2722–2727.
- [19] J. C. K. Laventall, "Coverage control by multi-robot networks with limited-range anisotropic sensory," *Int. J. Control*, vol. 82, pp. 1113–1121, 2009.
- [20] M. Zhu and S. Martínez, "Distributed coverage games for mobile visual sensor networks," *SIAM J. Control Optim.*, submitted for publication.
- [21] J. Cortés, S. Martínez, T. Karatas, and F. Bullo, "Coverage control for mobile sensing networks," *IEEE Trans. Robot. Autom.*, vol. 20, no. 2, pp. 243–255, Apr. 2004.
- [22] K. B. Ariyur and M. Krstic, *Real Time Optimization by Extremum Seeking Control*. New York: Wiley, 2003.
- [23] H.-H. Wang, S. Yeung, and M. Krstic, "Experimental application of extremum seeking on an axial-flow compressor," *IEEE Trans. Control Syst. Technol.*, vol. 8, no. 2, pp. 300–309, Mar. 1999.
- [24] H.-H. Wang and M. Krstic, "Extremum seeking for limit cycle minimization," *IEEE Trans. Autom. Control*, vol. 45, no. 12, pp. 2432–2436, Dec. 2000.
- [25] K. Stegath, N. Sharma, C. Gregory, and W. E. Dixon, "An extremum seeking method for non-isometric neuromuscular electrical stimulation," in *Proc. IEEE Int. Conf. Syst., Man Cybern.*, 2007, pp. 2528–2532.
- [26] D. Popovic, M. Jankovic, S. Magner, and A. Teel, "Extremum seeking methods for optimization of variable cam timing engine operation," *IEEE Trans. Control Syst. Technol.*, vol. 14, no. 3, pp. 398–407, May 2006.
- [27] Y. Ou, C. Xu, E. Schuster, T. C. Luce, J. R. Ferron, M. L. Walker, and D. A. Humphreys, "Design and simulation of extremum-seeking open-loop optimal control of current profile in the DIII-D tokamak," *J. Plasma Phys. Controlled Fusion*, vol. 50, no. 11, 2008, Fusion 50 115001.
- [28] Y. Tan, D. Nescic, and I. M. Mareels, "On non-local stability properties of extremum seeking controllers," *Automatica*, vol. 42, pp. 889–903, 2006.
- [29] J. Hale and S. V. Lunel, "Averaging in infinite dimensions," *Integr. Equations Appl.*, vol. 2, no. 4, pp. 463–494, 1990.
- [30] H. Khalil, *Nonlinear Systems*. Englewood Cliffs, NJ: Prentice-Hall, 2002.